

Electrically controllable magnetic order in the bilayer Hubbard model on honeycomb lattice — a determinant quantum Monte Carlo study

Jinhua Sun, Donghui Xu, Yi Zhou, and Fu-Chun Zhang

Department of Physics, Zhejiang University, Hangzhou, China
(Dated: June 24, 2021)

Layered antiferromagnetic spin density wave (LAF) state is one of the plausible ground states of charge neutral Bernal stacked bilayer graphene. In this paper, we use determinant quantum Monte Carlo method to study the effect of the electric field on the magnetic order in bilayer Hubbard model on a honeycomb lattice. Our results qualitatively support the LAF ground state found in the mean field theory. The obtained magnetic moments, however, are much smaller than what are estimated in the mean field theory. As electric field increases, the magnetic order parameter rapidly decreases.

PACS numbers: 73.22.Pr, 71.30.+h, 73.21.Ac, 75.75.-c

I. INTRODUCTION

Following the fabrication of monolayer graphene (MLG),¹ bilayer graphene (BLG) has attracted intensive attention due to its unique electrical flexibility^{2–5} and unusual physical properties such as unconventional integer quantum Hall effect (where the zero-level Hall plateau is missing).^{6,7} If we neglect electron-electron interactions, theoretical model for the bilayer graphene may be described by a tight-binding Hamiltonian, leading to parabolic valence and conduction bands touching at the highly symmetric Dirac points K and K' ,⁸ and a band gap may be opened by a perpendicular electric field, which saturates at $\sim 0.3eV$, as predicted and also observed in experiments.^{4,7,9,10}

Most recently, several well controlled experiments^{11–15} have demonstrated that an intrinsic gap of approximately 2meV may exist at the charge neutrality point (CNP) in ultraclean bilayer graphene. Bilayer graphene has finite density of states (DOS) at the CNP,¹⁶ which make it susceptible to the electron-electron interactions.^{17,18} Among various broken symmetry ground state candidates,^{19–32} the layered antiferromagnetic (LAF)^{26,28,33–36} spin density wave state is the most probable one. It is interesting to note that an electric field perpendicular to the graphene layers has been applied in experiments to control the physical properties. So far most theoretical works are based on mean field theories^{34,36–42} or renormalization group methods.^{23,27,28,36,39,41,43–45} Quantum Monte Carlo technique³⁶ has been used to study zero temperature properties in the absence of electric fields.

In this paper we use determinant quantum Monte Carlo (DQMC) method to study the effect of the electric field to a bilayer single band Hubbard model⁴⁶ on a honeycomb lattice, as shown in Fig. 1, relevant to bilayer graphene.

The DQMC method^{47,48} we adopt here has been used successfully to study interacting fermion problems. In this paper, we perform DQMC simulations to study the magnetic order at CNP and the behavior of order parameter when an perpendicular electric field is applied. The

DQMC results confirm a LAF ground state at CNP, and the magnetization monotonically decreases as the potential bias between the two layers increases. We also use the self-consistent mean-field analysis to draw the explicit results of critical values of electric potential when the system undergoes a transition from the LAF state to a layered charge polarized (LCP) state, with electron charge imbalance in the two layers and also on the two sublattices in the same layer.

The paper is organized as follows. In Sec. II, we give a brief introduction to our theoretical model and the physical quantities we study. In Sec. III, we present our results obtained from the DQMC simulations. Firstly, we study the magnetization at the CNP. The purpose is to identify the magnetic order at zero electric field. Then we proceed to discuss the suppression of the magnetization due to the electric field effect. In Sec. IV, we present the self-consistent mean-field results as a comparison and supplementary. Finally in Sec. V we summarize our results.

II. MODEL HAMILTONIAN

We utilize the Hubbard model to study electron interaction and magnetism in Bernal stacked bilayer graphene. In the presence of an external perpendicular electric field, the model Hamiltonian contains three parts, the kinetic energy H_0 , the on-site Coulomb repulsion H_U , and the electrostatic potential H_p induced by the external perpendicular electric field, and reads

$$H = H_0 + H_U + H_p. \quad (1)$$

Here the kinetic energy H_0 is given by

$$H_0 = -t \sum_{l\langle ij\rangle\sigma} [a_{l\sigma}^\dagger(i)b_{l\sigma}(j) + H.c.] - t_\perp \sum_{\langle ii'\rangle\sigma} [b_{1\sigma}^\dagger(i)a_{2\sigma}(i') + h.c.] - \mu \sum_{li\sigma} n_{li\sigma}(i), \quad (2)$$

where $a_{l\sigma}(i)$ ($b_{l\sigma}(i)$) annihilates an electron with spin σ at site i in sublattice A (B), $l = 1, 2$ is the layer index,

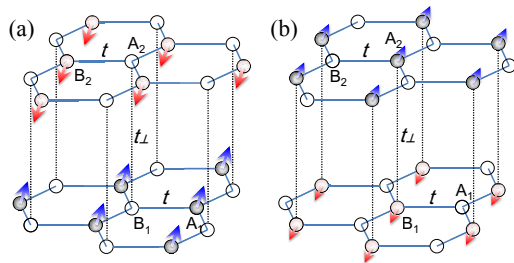


FIG. 1. (Color online). Bernal stacked bilayer graphene lattice and restricted AFM orders. A and B denote two sublattices. The subscripts 1 and 2 are layer indices. Intralayer hopping t links two nearest neighbor sites within the same layer, while interlayer hopping t_{\perp} links two nearest neighbor sites in opposite layers. The coordination number $z = 3$ for A₁ and B₂ sites, and $z = 4$ for A₂ and B₁ sites. (a) Restricted AFM order within $z = 3$ sites. (b) Restricted AFM order within $z = 4$ sites.

$\langle \dots \rangle$ denotes an intralayer or interlayer nearest neighbor bond as illustrated in Fig. 1. To be simple, we only take into account the nearest neighbor intralayer hopping t and the nearest neighbor interlayer hopping t_{\perp} . $n_{l\sigma}(i) = a_{l\sigma}^{\dagger}(i)a_{l\sigma}(i)$ or $(b_{l\sigma}^{\dagger}(i)b_{l\sigma}(i))$, depending on which sublattice (A or B) the site i belongs to. μ is the chemical potential, and $\mu = 0$ corresponds to the charge neutrality point. The on-site Hubbard interaction H_U can be written as

$$H_U = U \sum_{i\sigma} [n_{i\uparrow}(i) - 1/2][n_{i\downarrow}(i) - 1/2], \quad (3)$$

where $U > 0$ for the repulsion. The effect of the applied perpendicular electric field is parameterized by the potential difference V between the two layers,

$$H_p = \sum_{i\sigma} V_l n_{l\sigma}(i), \quad (4)$$

where $V_l = (-1)^l V/2$.

The intralayer nearest neighbor hopping t is estimated about $3.16eV$ in bilayer graphene. For convenience, we shall use t as the energy unit in our calculation. The interlayer nearest neighbor hopping t_{\perp} is commonly used as $0.381eV \sim 0.13t$ in literature. However, the effective parameters of bilayer graphene used in model studies are not given *a priori*, which is one of the roadblocks for determining the exact ground state of bilayer graphene. In this context, we would rather consider about more general situation: the parameters chosen are unrealistic, but more interesting than the real bilayer graphene parameter regime. In this paper, we shall consider two values for the interlayer hopping energy: $t_{\perp} = 0.2t$ and $1.0t$.

We close this section by providing an alternative site labeling scheme for the later use. Note that each unit cell in the Bernal stacked bilayer graphene contains four sites (two layers and two sublattices). The Bravais lattice for such a system is indeed a triangular lattice. Then one can denote a site as (\vec{R}, d) , where \vec{R} labels a unit cell and d labels the atom site within a unit cell, say, basis site. As would be seen in the next section, this Bravais lattice + basis parametrization is more convenience to study the magnetic order and correlation.

III. QUANTUM MONTE CARLO SIMULATIONS

We apply the DQMC method to study spin correlations and magnetic susceptibility in bilayer graphene, which avoids any assumption on the magnetic structure as in mean field theory or other approximations. In this sense, it is unbiased and numerically exact, namely, it is free of systematic errors but not random errors. DQMC evaluates the imaginary time Green's functions and thereby various correlation function through Wick's theorem at finite temperature.

As a finite temperature method, DQMC is able to examine different types of instability as temperature lowering. At first glance, this method is not applicable to catch possible long-ranged magnetic orders in the ground state. Since the Mermin-Wagner theorem⁴⁹ does not allow any long-ranged orders in the two dimensional Hubbard model at finite temperature. However, as pointed by Hirsch,⁴⁸ if we go to sufficiently low temperature where the thermal coherence length, or the thermal de Broglie wavelength is much larger than the linear system size, the system behaves as if it is at zero temperature. This makes DQMC able to catch ground state features in two dimension.

To study spin correlations and magnetic susceptibility in bilayer graphene, we choose the four-atom unit cell as discussed in the last paragraph in the last section. Thus both the spin structure factor and the spin susceptibility can be described by matrix elements of 4×4 matrices. The zz component of the static spin structure factor ($\omega = 0$) is defined as

$$S_{dd'}(\vec{q}) \equiv \frac{1}{L^2} \sum_{\vec{R}, \vec{R}'} e^{i\vec{q} \cdot (\vec{R} - \vec{R}')} \langle S_{\vec{R}d}^z \cdot S_{\vec{R}'d'}^z \rangle, \quad (5)$$

where L is the linear size of the Bravais lattice, thereby L^2 is the number of unit cells, and the total site number in the bilayer system is $N = 4L^2$. The indices d and d' denote the basis sites within a unit cell \vec{R} or \vec{R}' .

By diagonalizing the 4×4 matrix $S_{dd'}(\vec{q})$, we obtain the maximum eigenvalue $S(\vec{q})$. This spin structure factor $S(\vec{q})$ describe the dominant bilayer magnetic correlation at wave vector \vec{q} . We shall call it "dominant spin structure factor". Correspondingly, we can define a dominant magnetization (or staggered magnetization, depending

on the ground state) per site as follows,

$$m = \sqrt{S(q=0)/4L^2}.$$

Beside the dominant spin structure factor $S(\vec{q})$, we can also define the restricted structure factors for sites with coordination numbers $z = 3$ (A_1 and B_2) and $z = 4$ (B_1 and A_2),

$$S_z \equiv \frac{1}{2L^2} \sum_{i,j|z_i=z_j=z} \epsilon_{i,j} \langle S_i^z \cdot S_j^z \rangle, \quad (6)$$

from which we can obtain the local order parameters,

$$m_z = \sqrt{S_z/(2L^2)}.$$

If the two sites i and j belong to the same sublattice (A or B), then $\epsilon_{i,j} = 1$, otherwise $\epsilon_{i,j} = -1$. The corresponding magnetic orders are shown in Fig. 1(a) and Fig. 1(b) respectively.

Similarly, the static magnetic susceptibility is given by a 4×4 matrix,

$$\chi_{dd'}(\vec{q}) \equiv \frac{1}{L^2} \sum_{\vec{R}, \vec{R}'} e^{i\vec{q} \cdot (\vec{R} - \vec{R}')} \int_0^\beta \langle S_{\vec{R}d}^z(\tau) \cdot S_{\vec{R}'d'}^z \rangle. \quad (7)$$

The behavior of the largest eigenvalue of the matrix $\chi_{dd'}(\vec{q})$, $\chi(\vec{q})$, reveals the dominant magnetic response of the bilayer system.

As mentioned in previous section, we mainly consider two values of t_\perp in our calculations, (1) $t_\perp = 0.2t$ which is close to the realistic value of bilayer graphene and (2) $t_\perp = 1.0t$ where the symmetry breaking among the sublattices plays a more significant role. Using these parameters, we carry out DQMC calculation on $L \times L \times 4$ lattices up to $L = 9$ to study magnetic orders and fluctuations as the on-site Coulomb repulsion U and the interlayer bias V vary.

Again, we would like to emphasize that DQMC is a finite temperature method, according to Hirsch's argument⁴⁸, it can catch ground state features on finite size lattices only when the thermal coherence length is larger than the linear system size. For this purpose, we scale the temperature with the system size, and the temperature is chosen as $1/T = 1.2L$. $L = 9$ is the largest linear system size used in our DQMC simulations. The corresponding temperature is set as $T = 1/10.8$, which is about the lowest temperature we can approach without numerical instability.

III.1. Magnetic ordering in the absence of external electric field

Firstly, we would like to examine numerically the existence of magnetic order in the absence of external electric field. Only after that can we proceed to study the electric control of magnetic order in the bilayer graphene. In

order to do this, we calculate the dominant magnetization m and extrapolate it to the thermodynamic limit $L \rightarrow \infty$. A finite extrapolated value of m at thermodynamic limit indicates an magnetic ordered ground state. We present numerical results for $t_\perp = 1.0t$ and $t_\perp = 0.2t$ in Fig.2.

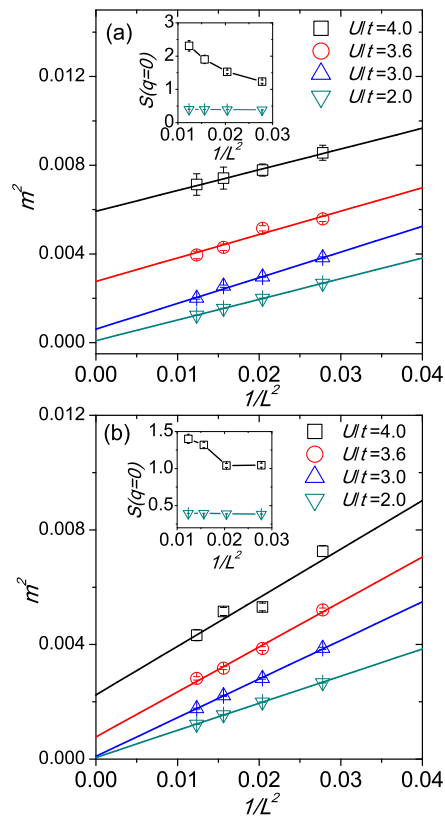


FIG. 2. (Color online). The dominant magnetization square m^2 is plotted as a function of $1/L^2$ for different values of U . Here we set $1/T = 1.2L$ and $V = 0$. (a) $t_\perp = 1.0t$, (b) $t_\perp = 0.2t$. The symbols are numerical results of DQMC simulations, and the lines are linear fitting. Insets: $S(q=0) = 4m^2L^2$ is plotted as a function of $1/L^2$, from which it is clear seen that $m(L \rightarrow \infty) = 0$ at $U/t = 2.0$.

As shown in Fig. 2 (a), when the interlayer hopping $t_\perp = 1.0t$, the dominant magnetization m vanishes at $U/t = 2.0$ but becomes finite at $U/t = 3.0, 3.6, 4.0$ in the thermodynamic limit. The critical point $U = U_c$ separating the magnetic ordered phase and the paramagnetic phase is in the range of $2.0t < U_c < 3.0t$. Fig. 2 (a) shows the results for weaker interlayer hopping $t_\perp = 0.2t$, which is close to the realistic value in bilayer graphene. It is clear that $3.0t < U_c < 3.6t$ when $t_\perp = 0.2t$. Comparing the estimated ranges for U_c at $t_\perp = 1.0t$ and $t_\perp = 0.2t$ as well as the absolute value of m , one finds that the inter-

layer hopping t_{\perp} favor magnetic ordering states and will enhance magnetic correlations. Since DQMC is a finite temperature method, thermal fluctuations will suppress the long ranged magnetic order, it must lowerestimate the value of m for ground state. But this deviation is not significantly when the temperature is much smaller than the energy gap. For $U = 4.0t$, the energy gap is about $0.3t$, the dominant magnetization we obtain by DQMC simulations at $T = 1/10.8$ is ~ 0.12 , which is in good agreement with that obtained by projector QMC at zero temperature.³⁶

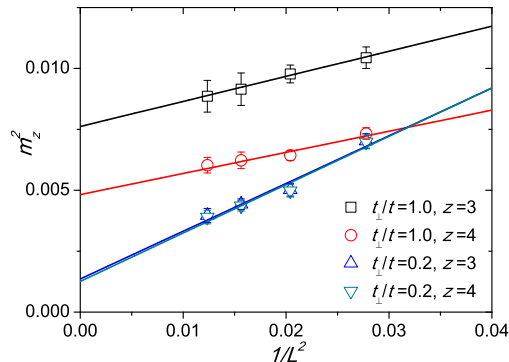


FIG. 3. (Color online). The restricted magnetization square m_z^2 in the absence of external electric field is plotted as a function of $1/L^2$. Here we set $U = 4.0t$.

Moreover, we can specify the magnetic structure by studying the local order parameters m_z . As shown in Figs. 1(a) and 1(b), $m_{z=3}$ is the staggered magnetization in the $z = 3$ sublattices (A_1 and B_2), while $m_{z=4}$ is the staggered magnetization in the $z = 4$ sublattices (A_2 and B_2). The later two sublattices ($z = 4$) are linked by the interlayer hopping t_{\perp} . As plotted in Fig. 3, for $V = 0$ and $U = 4.0t$, both staggered magnetization $m_{z=3}$ and $m_{z=4}$ exist when $t_{\perp} = 0.2t$ or $t_{\perp} = 1.0t$. For $t_{\perp} = 0.2t$, the values of $m_{z=3}$ and $m_{z=4}$ almost coincide each other, while for $t_{\perp} = 1.0t$, $m_{z=4}$ is apparently smaller than $m_{z=3}$ although both $m_{z=4}$ and $m_{z=3}$ are larger than their values at $t_{\perp} = 0.2t$.

The similarity and difference between $t_{\perp} = 0.2t$ and $t_{\perp} = 1.0t$ can be explained as follows. Both $m_{z=3}$ and $m_{z=4}$ reflect antiferromagnetic spin correlation between the two layers. Increasing t_{\perp} will enhance this correlation directly or indirectly, thus both $m_{z=3}$ and $m_{z=4}$ will increase with t_{\perp} as seen in Fig. 3. However, the other tendency induced by the hopping terms (both t and t_{\perp}) is to against the on-site Coulomb repulsion U and drive the electrons to be itinerant rather than localized. This will reduce the magnitude of local magnetic moment effectively. Therefore the magnitude of the local moment at $z = 4$ sites becomes smaller than that at $z = 3$ sites, resulting in $m_{z=4} < m_{z=3}$.

III.2. Magnetic orders and fluctuations in the presence of external perpendicular electric field

Now we turn on the external perpendicular electric field to see its effect on the LAF states. In bilayer graphene, experimentally tunable bias V is up to about $1.0t$. In principle, we can use larger V in theoretical study. However, our DQMC simulation will suffer from serious negative sign problem when $V > 1.0t$, see Appendix for details. We find that the dominant magnetization m will be suppressed by the external perpendicular electric field. The numerical results are summarized in Fig. 4. We fix $U = 4.0t$ and focus on two values of t_{\perp} , $1.0t$ and $0.2t$, where LAF order is well established in the absence of external electric field. Fig. 4 exhibits clear tendency that long ranged magnetic order will be suppressed by the perpendicular electric field. However, $V = 1.0\text{eV}$, which is the maximum value approachable by our DQMC simulation, is still insufficient to destroy the magnetic ordering entirely. We shall apply the mean field theory to study the possible transition from the LAF ordered phase to the paramagnetic phase in the next section for completeness.

Magnetic fluctuations are investigated through the temperature dependent static spin susceptibility $\chi(\vec{q} = 0)$. We still set $U = 4.0t$ and study the cases of $t_{\perp} = 1.0t$ and $t_{\perp} = 0.2t$. It is shown in Fig. 5 that the magnetic susceptibility χ will diverge at $V = 0$ as temperature $T \rightarrow 0$. This instability will give rise to magnetic ordering at zero temperature. As the potential bias V increases, the magnetic susceptibility χ will be gradually suppressed.

From Fig. 4 and Fig. 5, one sees that both magnetic ordering and magnetic fluctuations are suppressed by the applied perpendicular electric field. This means that the magnitude of local magnetic moment is reduced. The reduction of local moment can be explained as follows. At half filling, the average electron occupation number per site is unit. The perpendicular electric field will increase the electron occupation number on one layer and decrease that on the other layer, resulting in reduced local moment. This is in agreement with the deviation of electron occupation number from the unit as shown in the insets in Fig. 4. We shall also examine this argument through mean field theory in next section.

IV. MEAN FIELD THEORY

In order to go beyond the limit of DQMC, where the reliable results can be obtain only when $V < 1.0t$ due to sign problem, we carry out mean field analysis to investigate possible phase transition from the SDW state to paramagnetic state as V increases. Following Ref.³⁴, we introduce the following mean field decomposition for the

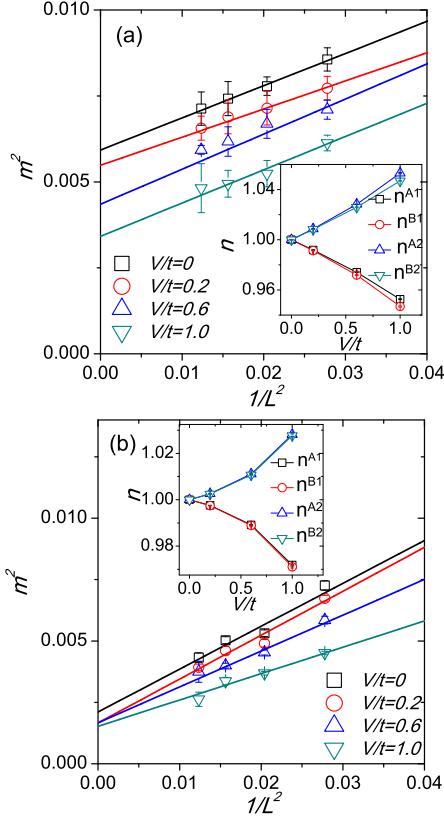


FIG. 4. (Color online). The dominant magnetization square m^2 is plotted as a function of $1/L^2$ in the presence of external perpendicular electric field. Here we set $U = 4.0t$. (a) $t_{\perp} = 1.0$, (b) $t_{\perp} = 0.2$. Insets: The electron occupation numbers in four sublattices.

Coulomb interaction term,

$$H_U^{MF} = U \sum_{l,\sigma} [(\langle n_{l\sigma}(i) \rangle - 1/2)(n_{l\bar{\sigma}}(i) - 1/2)], \quad (8)$$

where $\bar{\sigma} = -\sigma$, and $\langle n_{l\sigma}(i) \rangle$ should be determined self-consistently. To describe LAF spin density wave states, we introduce eight mean fields $\langle n_{l\sigma}^{\eta} \rangle$ for $\langle n_{l\sigma}(i) \rangle$, where η indicates the sublattice A or B. Then local magnetization and electron occupation number at each carbon atom site can be defined in terms of $\langle n_{l\sigma}^{\eta} \rangle$ respectively,

$$m_l^{\eta} = \frac{1}{2} \langle n_{l\uparrow}^{\eta} - n_{l\downarrow}^{\eta} \rangle \quad (9)$$

and

$$n_l^{\eta} = \langle n_{l\uparrow}^{\eta} + n_{l\downarrow}^{\eta} \rangle. \quad (10)$$

We choose $t_{\perp} = 1.0t$ and $U = 4.0t$ to study how the magnetization will be reduced and how charge imbalance

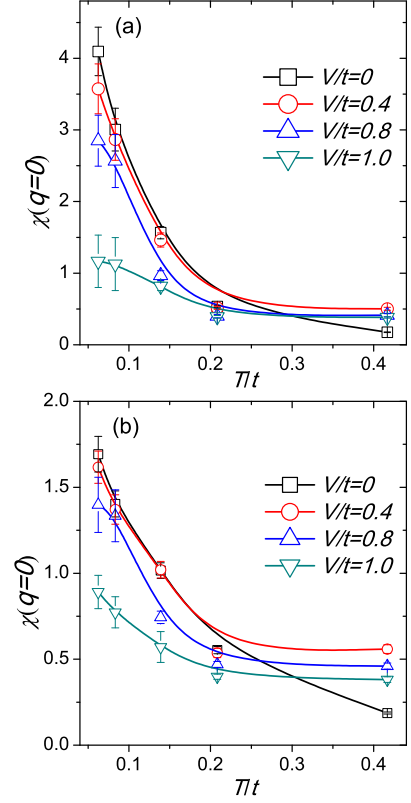


FIG. 5. (Color online). The spin susceptibility χ as a function of T in the presence of external perpendicular electric field. Here we set $U = 4.0t$. (a) $t_{\perp} = 1.0$, (b) $t_{\perp} = 0.2$.

between the two layers will be induced as the potential bias V increasing. The mean field results are shown in Fig. 6(a) and 6(b).

When $V = 0$, the ground state is a gapful LAF state. As shown in Fig. 6(a), the magnitude of the magnetization at $z = 3$ sites (A_1 and B_2) is larger than that at $z = 4$ sites (A_2 and B_1), which is consistent with DQMC results (see Fig. 3). However, the magnitude of the magnetization given by mean field theory is bigger than those in DQMC simulation. This is because of two reasons. Firstly, DQMC is a finite temperature method, thermal fluctuations are involved, which will reduce order parameters on the ground state. Secondly, the mean field theory neglects the quantum fluctuations and tends to overestimate the magnetization.

As the potential bias V increasing, the system experiences continuous charge transfer from one layer to the other as shown in 6(b). This charge transfer will induce charge imbalance between the two layers. Since t_{\perp} only links sublattices A_2 and B_1 , it will also induce charge imbalance between sublattices A and B. The charge transfer will also reduce the local magnetic moment effectively.

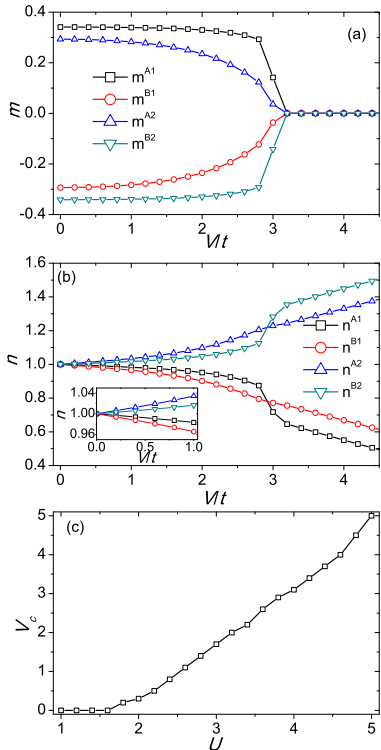


FIG. 6. (Color online). (a) The mean field results of magnetization m and (b) charge number for $U = 4.0t$ and $t_{\perp} = 1.0t$ as a function of potential bias V . Here we use $U = 4.0$. Inset: A zoom for the charge number at the range of $0 < V < 1.0t$. (c) The critical potential bias V_c for various values of U for $t_{\perp} = 1.0t$.

The larger charge imbalance (measured from single occupancy) corresponds to smaller local moment. In the large V limit, the system becomes a paramagnetic and layered charge polarized state. The phase transition from LAF to paramagnetic state happens at $V = V_c \approx 3.2t$.

It is interesting that although the charge imbalance between two layers and two sublattices drives each site away from single occupancy, the relation

$$n^{A1} + n^{B2} = n^{B1} + n^{A2} = 2.0 \quad (11)$$

still keeps up. This relation can be explained by a combined symmetry. Although the external electric field breaks the charge conjugation (or particle-hole) symmetry as well as the lattice inversion symmetry, the combination of the charge conjugation and the lattice inversion is still a symmetry operation under the external electric field. This combined charge-conjugation-lattice-inversion symmetry will guarantee Eq. (11).

Finally, we fix the interlayer hopping $t_{\perp} = 1.0t$ and vary on-site Coulomb repulsion U to study the critical

values of V , which separates the LAF phase and the paramagnetic phase. The mean field results are present in Fig. 6 (c). By the mean field theory, the system starts to develop the magnetization at $U \sim 1.8t$. Thus the value V_c makes sense only when $U > 1.8t$. In Fig. 6 (c), one sees that V_c increases monotonically with U , and the increasing becomes faster when $U > 4.0t$. V_c is mainly determined by the spin density wave (SDW) gap opened by U . Since the SDW gap increases exponentially with U near U_c ,³⁶ we expect that V_c will also grows nearly exponentially with U .

V. DISCUSSION AND CONCLUSION

In conclusion, we have studied the effect of external potential bias on the magnetization in the bilayer honeycomb lattice Hubbard model. Two typical values of interlayer hopping energy are tested: $t_{\perp} = 0.2t$, which is close to the value in bilayer graphene with Bernal stacking; and $t_{\perp} = 1.0t$, which represents a larger interlayer coupling. In the absence of a potential bias in the bilayer system, there is a layered antiferromagnetic order at $U > 3.0t$. The magnetization on the sites connected by the interlayer hopping "bonds" is suppressed by the interlayer hopping, while the magnetization on other sites is slightly enhanced by the interlayer hopping. For both $t_{\perp} = 1.0t$ and $0.2t$, both of the DQMC results and the mean-field analysis support the LAF ground state. In the presence of a perpendicular electric field, the antiferromagnetic order is suppressed. Due to the negative sign problem, we are not able to approach large values of potential bias and to obtain the critical value V_c for the transition from an antiferromagnetic to paramagnetic states in the DQMC simulation. However, the tendency of decreasing magnetization as V increases is clearly observed in the QMC results, and the critical value V_c for various values of U is explicitly given by the self-consistent mean-field analysis.

VI. ACKNOWLEDGEMENT

This work is supported in part by National Basic Research Program of China (No.2011CBA00103/2014CB921201/2014CB921203), NSFC (No.11374256/11274269), and the Fundamental Research Funds for the Central Universities in China.

Appendix A: On negative sign problem

In a Monte Carlo simulation, we evaluate the expectation value of a quantity A as follows,

$$\langle A \rangle_p = \frac{\sum_i p_i A_i}{\sum_i p_i}, \quad (A1)$$

where $\sum_i p_i > 0$. If $p_i > 0$, it serves a "Boltzmann weight" and describes a distribution. Then one can use

the distribution p to evaluate the expectation value $\langle A \rangle$ by Monte Carlo method. However, sometimes p_i is not positive definite, namely, $p_i < 0$ occurs. In this case, p_i is no longer a distribution function. But one can still rewrite $\langle A \rangle_p$ in Eq. (A1) as

$$\langle A \rangle_p = \frac{\sum_i p_i A_i \sum_i |p_i|}{\sum_i |p_i| \sum_i p_i} = \frac{\langle sA \rangle_{p'}}{\langle s \rangle_{p'}}, \quad (\text{A2})$$

where $p' = |p|$ and $s_i = p_i/|p_i|$ is the sign of p_i . The one can evaluate two expectation values $\langle sA \rangle_{p'}$ and $\langle s \rangle_{p'}$ by Monte Carlo method under the distribution p' .

If $\langle s \rangle_{p'}$ is sizable and much larger than the statistical

error bar, the Monte Carlo simulation is still efficient. However, when $\langle s \rangle_{p'} \ll 1$, the strong statistical fluctuation cannot be compensated by longer Monte Carlo runs. This is so called “negative sign problem”. Actually, it has been confirmed that the average sign has the relation $\langle s \rangle \sim e^{-\beta N \gamma}$, where γ depends on the filling n and interaction U . In our calculation, as the system size grows, and as the potential bias increases, the negative sign problem becomes quite serious. For example, while $t_{\perp} = 1.0t$, $U = 4.0t$ and $T = 1/10.8$, the sign average $\langle s \rangle \sim 0.1$ for $V = 1.0t$ when the system size is $N = 9 \times 9 \times 4$.

-
- ¹ K. S. Novoselov, A. K. Geim, S. V. Morozov, D. Jiang, Y. Zhang, S. V. Dubonos, I. V. Grigorieva, and A. A. Firsov, *Science* **306**, 666 (2004).
- ² E. V. Castro, K. S. Novoselov, S. V. Morozov, N. M. R. Peres, J. M. B. L. dos Santos, J. Nilsson, F. Guinea, A. K. Geim, and A. H. C. Neto, *Phys. Rev. Lett.* **99**, 216802 (2007).
- ³ J. Oostinga, H. Heersche, X. Liu, A. Morpurgo, and L. Vandersypen, *Nature Materials* **7**, 151 (2008).
- ⁴ Y. Zhang, T.-T. Tang, C. Girit, Z. Hao, M. Martin, A. Zettl, M. Crommie, Y. Shen, and F. Wang, *Nature* **459**, 820 (2009).
- ⁵ K. F. Mak, C. H. Lui, J. Shan, and T. F. Heinz, *Phys. Rev. Lett.* **102**, 256405 (2009).
- ⁶ K. Novoselov, E. McCann, S. Morozov, V. Fal’ko, M. Katsnelson, U. Zeitler, D. Jiang, F. Schedin, and A. Geim, *Nature Physics* **2**, 177 (2006).
- ⁷ E. McCann and V. I. Fal’ko, *Phys. Rev. Lett.* **96**, 086805 (2006).
- ⁸ A. H. Castro Neto, F. Guinea, N. M. R. Peres, K. S. Novoselov, and A. K. Geim, *Rev. Mod. Phys.* **81**, 109 (2009).
- ⁹ T. Ohta, A. Bostwick, T. Seyller, K. Horn, and E. Rotenberg, *Science* **313**, 951 (2006).
- ¹⁰ H. Min, B. Sahu, S. K. Banerjee, and A. H. MacDonald, *Phys. Rev. B* **75**, 155115 (2007).
- ¹¹ J. Velasco Jr., L. Jing, W. Bao, Y. Lee, P. Kratz, V. Aji, M. Bockrath, C. Lau, C. Varma, R. Stillwell, D. Smirnov, F. Zhang, J. Jung, and A. MacDonald, *Nature Nanotechnology* **7**, 156 (2012).
- ¹² F. Freitag, J. Trbovic, M. Weiss, and C. Schönenberger, *Phys. Rev. Lett.* **108**, 076602 (2012).
- ¹³ A. Veligura, H. J. van Elferen, N. Tombros, J. C. Maan, U. Zeitler, and B. J. van Wees, *Phys. Rev. B* **85**, 155412 (2012).
- ¹⁴ F. Freitag, M. Weiss, R. Maurand, J. Trbovic, and C. Schönenberger, *Phys. Rev. B* **87**, 161402 (2013).
- ¹⁵ W. Bao, J. Velasco Jr., F. Zhang, L. Jing, B. Standley, D. Smirnov, M. Bockrath, A. MacDonald, and C. Lau, *Proc. Natl. Acad. Sci. U. S. A.* **109**, 10802 (2012).
- ¹⁶ E. V. Castro, M. P. Lopez-Sancho, and M. A. H. Vozmediano, *New J. Phys.* **11**, 095017 (2009).
- ¹⁷ K. Sun, H. Yao, E. Fradkin, and S. A. Kivelson, *Phys. Rev. Lett.* **103**, 046811 (2009).
- ¹⁸ S. Uebelacker and C. Honerkamp, *Phys. Rev. B* **84**, 205122 (2011).
- ¹⁹ J. Nilsson, A. H. Castro Neto, N. M. R. Peres, and F. Guinea, *Phys. Rev. B* **73**, 214418 (2006).
- ²⁰ H. Min, G. Borghi, M. Polini, and A. H. MacDonald, *Phys. Rev. B* **77**, 041407 (2008).
- ²¹ R. T. Weitz, M. T. Allen, B. E. Feldman, J. Martin, and A. Yacoby, *Science* **330**, 812 (2010).
- ²² R. Nandkishore and L. Levitov, *Phys. Rev. Lett.* **104**, 156803 (2010).
- ²³ O. Vafek and K. Yang, *Phys. Rev. B* **81**, 041401 (2010).
- ²⁴ O. Vafek, *Phys. Rev. B* **82**, 205106 (2010).
- ²⁵ F. Zhang, H. Min, M. Polini, and A. H. MacDonald, *Phys. Rev. B* **81**, 041402 (2010).
- ²⁶ F. Zhang, J. Jung, G. A. Fiete, Q. Niu, and A. H. MacDonald, *Phys. Rev. Lett.* **106**, 156801 (2011).
- ²⁷ Y. Lemonik, I. Aleiner, and V. I. Fal’ko, *Phys. Rev. B* **85**, 245451 (2012).
- ²⁸ M. M. Scherer, S. Uebelacker, and C. Honerkamp, *Phys. Rev. B* **85**, 235408 (2012).
- ²⁹ V. N. Kotov, B. Uchoa, V. M. Pereira, F. Guinea, and A. H. Castro Neto, *Rev. Mod. Phys.* **84**, 1067 (2012).
- ³⁰ M. Kharitonov, *Phys. Rev. B* **85**, 155439 (2012).
- ³¹ E. V. Gorbar, V. P. Gusynin, V. A. Miransky, and I. A. Shovkovy, *Phys. Rev. B* **86**, 125439 (2012).
- ³² F. Zhang, H. Min, and A. H. MacDonald, *Phys. Rev. B* **86**, 155128 (2012).
- ³³ F. Zhang and A. H. MacDonald, *Phys. Rev. Lett.* **108**, 186804 (2012).
- ³⁴ D.-H. Xu, J. Yuan, Z.-J. Yao, Y. Zhou, J.-H. Gao, and F.-C. Zhang, *Phys. Rev. B* **86**, 201404 (2012).
- ³⁵ Y. Wang, H. Wang, J.-H. Gao, and F.-C. Zhang, *Phys. Rev. B* **87**, 195413 (2013).
- ³⁶ T. C. Lang, Z. Y. Meng, M. M. Scherer, S. Uebelacker, F. F. Assaad, A. Muramatsu, C. Honerkamp, and S. Wessel, *Phys. Rev. Lett.* **109**, 126402 (2012).
- ³⁷ E. R. Jinhua Zhang, Rahul Nandkishore, , arXiv:1401.0727.
- ³⁸ J. Yuan, D.-H. Xu, H. Wang, Y. Zhou, J.-H. Gao, and F.-C. Zhang, *Phys. Rev. B* **88**, 201109 (2013).
- ³⁹ O. V. James M. Murray, , arXiv:1312.6831v1.
- ⁴⁰ X.-Z. Yan and C. S. Ting, *Phys. Rev. B* **86**, 235126 (2012).
- ⁴¹ V. Cvetkovic, R. E. Throckmorton, and O. Vafek, *Phys. Rev. B* **86**, 075467 (2012).
- ⁴² M. Kharitonov, *Phys. Rev. B* **86**, 195435 (2012).

- ⁴³ M. M. Scherer, S. Uebelacker, D. D. Scherer, and C. Honerkamp, *Phys. Rev. B* **86**, 155415 (2012).
- ⁴⁴ K. W. Song, Y.-C. Liang, and S. Haas, *Phys. Rev. B* **86**, 205418 (2012).
- ⁴⁵ F. Zhang, H. Min, and A. H. MacDonald, *Phys. Rev. B* **86**, 155128 (2012).
- ⁴⁶ J. Hubbard, Proceedings of the Royal Society of London. Series A, Mathematical and Physical Sciences **276**, 4403 (1963).
- ⁴⁷ R. Blankenbecler, D. J. Scalapino, and R. L. Sugar, *Phys. Rev. D* **24**, 2278 (1981).
- ⁴⁸ J. E. Hirsch, *Phys. Rev. B* **31**, 4403 (1985).
- ⁴⁹ N. D. Mermin and H. Wagner, *Phys. Rev. Lett.* **17**, 1133 (1966).